



Ultra-high areal capacity, ultra-long life, dendrite-free sodium metal anode enabled by antimony-based Na-ion conducting artificial SEI layers

Megala Moorthy^a, Ranjith Thangavel^b, Bala Krishnan Ganesan^a, Aditi Saha^c,
Seungbum Hong^c, Yun-Sung Lee^{a,*}

^a School of Chemical Engineering, Chonnam National University, Gwangju 61186, Republic of Korea

^b School of Energy Science and Engineering, Indian Institute of Technology Guwahati, Guwahati 781039, India

^c Department of Materials Science and Engineering, Korea Advanced Institute of Science and Technology (KAIST) Daejeon, 34141, Republic of Korea

ARTICLE INFO

Keywords:

Na metal anode
Dendrites
Solid state battery
Artificial interface
Mechanical strength

ABSTRACT

Sodium metal (Na) is a promising anode material for Na metal batteries and solid-state sodium batteries, because of its high theoretical capacity, favorable electrochemical potential, and cost effectiveness. Nevertheless, practical applications of sodium metal anode are hindered by uncontrolled dendrite growth owing to chemical instability of the heterogeneous solid electrolyte interphase layer. In this work, we proposed a simple interface modification strategy employing several antimony-based Na-ion conducting solid electrolyte complexes as protective artificial SEI layer over Na metal. The Na-ion conducting interphases are robust and highly Na-ion conductive to attain uniform sodium ion flux with a small overpotential. Importantly, Na anode with antimony sulfide based solid electrolyte SEI layers exhibited the high-rate performance (10 mA cm^{-2}) along with a remarkable capacity of 30 mAh cm^{-2} , and life span of $\sim 1100 \text{ h}$. We observe that replacing the conventional artificial SEI layers, employing alloy type interface with Na-ion conducting solid electrolyte as artificial SEI components will improve the mechanical robustness at high current and high-capacity conditions. The sodium metal batteries employing modified metal anodes and high voltage $\text{Na}_{1.2}\text{Mn}_{0.8}\text{O}_{1.5}\text{F}_{0.5}$ cathode, exhibited excellent stability and high efficiency at 1C rate. Furthermore, the modified metal anodes are well-compatible with Na_3SbS_4 solid-state electrolyte, and the symmetrical solid-state battery exhibited a stable interface. Our strategy holds significant promise and has the potential for widespread application in the advancement of high-energy sodium metal batteries and solid-state sodium batteries.

1. Introduction

In the realm of smart electronic gadgets and electric automobiles, their performance significantly depends on the energy efficiency of the embedded battery. The escalating demand for portable electronic devices has spurred considerable research on the development of high-energy-density rechargeable batteries [1,2]. Among the various types of alkali-ion batteries, including lithium, sodium-and potassium-ion batteries, sodium-ion batteries (SIB) have emerged as a promising candidate for affordable smart energy storage [3,4]. In recent years, battery researchers around the world have diligently explored various electrode materials for SIBs. Among these materials, hard carbon anodes have exhibited promising outcomes. However, their constrained theoretical capacity in SIBs has significantly limited the advancement of next-generation battery technology. In contrast to lithium-ion batteries,

the substitution of commercial graphite anodes in sodium-ion battery is not feasible because of the large atomic radius of sodium, which hinders practical storage of sodium ions within the graphite structure [5–7]. In recent years, among all the materials explored for anodes, sodium metal has emerged as a highly promising anode material for high-energy sodium batteries, because of its high theoretical capacity (1166 mAh g^{-1}), reasonable electrochemical potential (-2.71 vs SHE), and low weight (0.968 g cm^{-3}) with high abundance [8,9]. However, in practice, the use of sodium metal anode is limited, due to the uncontrolled sodium dendrite growth formation during repeated plating/stripping cycles, resulting in low coulombic efficiency and shorter lifespan. This uncontrolled sodium ion deposition occurs primarily at the metal/electrolyte interfaces, and it is attributed to the uneven solid electrolyte interphase (SEI) layer [10–13]. As the number of cycles increases, heterogeneous nucleation with Na metal worsens, and also uneven local electric fields

* Corresponding author.

E-mail address: leeyes@chonnam.ac.kr (Y.-S. Lee).

<https://doi.org/10.1016/j.cej.2024.155234>

Received 23 May 2024; Received in revised form 13 August 2024; Accepted 26 August 2024

Available online 27 August 2024

1385-8947/© 2024 Published by Elsevier B.V.

that have already been triggered. Furthermore, sodium dendrites can easily penetrate the separator and reach the cathode, leading to short circuits [14–16].

In particular, the establishment of an artificial SEI layer on sodium metal has emerged as the most promising and primary approach to regulate and stabilize the uncontrolled sodium ion nucleation behavior on sodium metal [17–19]. Also, various strategies such as, nanocarbon skeletons, Mxene layers, Na-alloy interfaces, metal oxides, organic polymers and sodio-philic matrix have been utilized as interface/artificial SEI layer for Na metal anodes [6,20,21]. Unlike the naturally occurring SEI, an artificially engineered SEI exhibits a markedly smoother surface and enhanced mechanical resilience, leading to the uniform deposition of sodium ions [22]. Irrespective of the significant advancement in the artificial SEI layers, the capacity of Na metal deposited, and current density of facile Na metal deposition is still limited, far behind the requirement. It is mainly attributed to poor mechanical stability of the artificial SEI layer employed of the metal anode. The sodium storage capacity, and the current density of the several artificial SEI layer coated Na metal anode is in the range of 1–10 mAh cm⁻², and 1–5 mA cm⁻² respectively, limiting the energy output and power density of the metal batteries [23,24].

Utilizing Na-ion solid electrolyte over Na metal as artificial SEI layer can have a several advantages over conventional artificial SEI layers. The use of a single ion conducting solid-state electrolyte as the protection layer can improve the ionic conductivity of SEI layer with minimal side reactions towards electrolyte [25]. The Na-ion conducting inorganic solid electrolytes are known to have sufficient mechanical strength to prevent cracking, and deformation that help to overcome severe volume changes. Among the various solid-state electrolytes, chalcogenide-based Na-ion conducting electrolytes have attracted considerable attention owing to their high ionic conductivity (10⁻⁴–10⁻² S cm⁻¹) and high electronic resistivity at room temperature [26]. The faster Na-ion diffusion in chalcogenide-based conducting framework is intrinsically high owing to the smaller ionic radius of sulfide anion and weaker electrostatic force between the anionic framework and Na-ions because of the low electronegativity of anion (sulfur) atoms [27]. Moreover, they exhibit lower grain boundary resistance and better intimate contact, helping to lower the interfacial resistance and increase the Na-ion diffusion kinetics. Several works have previously studied the direct casting of solid electrolyte over Li metal anode, and Na metal anode as artificial SEI layer [18,28,29]. Although, the kinetics and performance of those modified anodes are better than pristine metal anode.

Herein, we report the issues in Na metal anode by developing Na-ion conducting complex containing a combination of Na₃SbS₄ solid electrolyte, Na₃Sb alloy, and inorganic components as hybrid protective artificial SEI layer through a facile in-situ reaction strategy. The antimony-based solid electrolytes (Na₃SbS₄) can be a promising candidate for enhancing facile Na-ion transport over Na metal anode and the sodium-rich antimony interphases can deliver a stable and low charge transfer resistance, and thereby facilitating rapid sodium ion transportation and effectively mitigate side reactions [19,30]. The controlled reaction between the Na-metal and solid electrolyte components generates a Na-ion conducting solid electrolyte interphase near the sodium metal anode, can significantly reduce the resistance between the Na metal and the electrolyte. The hybrid artificial SEI layer exhibits the capability to control sodium-ion flux, leading to the uniform deposition of sodium while minimizing overpotential. Na metal anodes with Na₃SbS₄ protective SEI layer can be cycled over 1100 h in a symmetrical cell with low overpotential (10 mV), and high-rate performance (10 mA cm⁻²) along with a remarkable capacity of 30 mAh cm⁻², higher than pristine Na metal (60 mV after 120 h). The Na anodes with in-situ generated solid electrolyte as artificial SEI has greater reversibility with reduced polarization compared to those of pristine Na metal.

We have also investigated the effect of anion on solid electrolyte complex by replacing S with I and F complexes. The anions strongly

influence the solid electrolyte formation ability over the Na metal, directly influencing the ionic conductivity, and mechanical strength of the artificial SEI interface, and the components of SEI layer. The sodium metal battery studied by coupling with high voltage Na_{1.2}Mn_{0.8}O_{1.5}F_{0.5} cathode, and the modified anode achieves extremely high coulombic efficiency, and extended cycle life than pristine Na metal anode. Moreover, the solid-state battery employing modified anode and Na₃SbS₄ solid-state electrolyte depicted excellent interface compatibility. This work offers a cost-effective solution and opens new avenues for designing low-cost, long-cycle-life anodes that can be used in high-energy sodium metal batteries, and solid-state batteries.

2. Experimental section

2.1. Materials

In the synthesis process, we utilized pure Na metal cubes (Sigma Aldrich, purity of 99.9 %), antimony sulfide (Sb₂S₃, Sigma Aldrich, purity of 98 %), antimony iodide (SbI₃, Sigma Aldrich, purity of 99 %), antimony fluoride (SbF₃, Sigma Aldrich, purity of 99 %), and THF solvent (THF, Junsei Chemical). All these chemicals were sourced from South Korea, and they were stored in a glove box filled with argon gas. The moisture level in the glove box was maintained at less than 0.1 ppm throughout the storage period to avoid exposing highly reactive sodium to air and moisture and also to ensure the purity and integrity of the chemicals.

2.2. Construction of antimony-based interphase layers

All experimental procedures, including the preparation of the metal alloy solutions and fabrication of electrodes, were conducted within the argon glove box to maintain a controlled and sensitive testing environment. The metal alloy solution to be deposited onto sodium (Na) metal anodes was formulated by, initially dissolving a metal salt (Sb₂S₃), such in THF by continuous mixing. Before the artificial SEI layer formation on metal anode by chemical reaction of metal salt containing solution, bulk Na metal was subjected to initial processing, which involved cutting to remove excess oxide layers and continuous rolling to achieve a flat surface. Subsequently, the Na metal was cut into 11-mm diameter and then the prepared Sb salt containing THF solution were applied on Na metal by simple drop-casting method. The resulting Na electrodes were kept separately and dried within the glove box. Notably, all the electrodes used for comparison were prepared in the same manner and subjected to comprehensive physical, chemical and electrochemical characterization.

2.3. Characterization of materials

Crystal-phase data of the electrodes were inferred from X-ray diffraction (XRD) patterns, which were recorded using a high-resolution 3D X-ray diffractometer (Pan Analytical) equipped with a Cu K α radiation source operated at 1.8 KW (max, 60 KW, 55 mA). To record surface and cross-sectional view of both fresh Na and protected antimony-based interphase electrodes, using a field emission scanning electron microscope (FE-SEM–S-4700/EX-200). This study allowed to obtain detailed insights into their morphologies. To perform elemental composition analysis, utilized an energy-dispersive X-ray spectrometer (EDS) integrated with the SEM, and to prevent exposure of sodium to the atmosphere, all samples were securely stored in airtight containers. The SEI layers compositions and their oxidation states were investigated using an ultra-high-vacuum scientific X-ray photoelectron spectroscope (Thermo VG). To maintain the integrity of the analysis and minimize the potential for surface reactions, all the samples were promptly placed in a closed container and rapidly transferred to the spectroscopy chamber. This rapid and careful handling was crucial in ensuring the accuracy and dependability of spectroscopic analysis. AFM study was investigated by

using commercial atomic force microscope (MFP-3D Origin, set up with electrically closed cell, Oxford Instruments Asylum Research Inc., USA). For both topography and nanoindentation measurements, a diamond tip (DT-NCHR) and a spring constant of 80 N/m were used. Young's modulus values for both pristine Na and SSE-based electrode were calculated using the Hertzian model calculation with a 3 μN applied force over a surface area of $10 \times 10 \mu\text{m}$.

2.4. Electrochemical characterization

To study the mechanism underlying the Na storage performance, and to evaluate electrochemical performance of the pristine Na and modified anodes, CR2032 coin cells were assembled in a glove box. Galvanostatic plating/stripping tests of the electrodes were performed at room temperature by using a Battery Cycler-3000 (WonATech), to assess their responses by varying capacities ranging from 2 mAh to 30 mAh cm^{-2} at a constant current density of 2 mA cm^{-2} . Additionally, a potentiostat workstation (Biologic) was to perform electrochemical impedance spectroscopy (EIS) analysis in the frequency range of 200 KHz to 100 mHz for obtaining insights into the charge transfer processes. In all symmetric cell tests, fresh sodium foil and the modified electrodes served as the working and counter electrodes, respectively. Subsequently, advanced to the full cell assembly modified Na anode and $\text{Na}_x\text{Mn}_{2-x}\text{O}_{1.5}\text{F}_{0.5}$ (NMF) as the cathode was used. The physical and electrochemical performance of cathode materials were studied previously by our research group [31]. The NMF electrode material, formulated in a ratio of 70:20:10 (active material: carbon black: polyvinylidene difluoride (PVDF)) was dissolved in N-methyl-2-pyrrolidone (NMP) solvent. This slurry was then coated onto an aluminum foil current collector and dried for 12 h and the mass loading of the cathode is 1.5 mg cm^{-2} . Subsequent galvanostatic charge–discharge studies of the full cells were conducted using the battery cycler (Wona-Tech) in a voltage window of (1.5–3.8 V vs. Na^+). The electrolyte used in all investigations consisted of 1 M NaPF_6 , dissolved in diglyme solvent. Each cell was equipped with a 15- μm -thick polypropylene separator to facilitate the electrochemical processes. For SSBs, Na-Na symmetric cell was constructed within the CR2032 coin cell by sandwiching the solid state electrolyte pellet between pristine Na and modified Na metal electrode separately as discussed in our previous work [32].

3. Results and discussion

The Na-ion conducting solid electrolyte type protective artificial SEI layer was created over Na metal surface by a facile self-chemical

reduction reaction between Na metal and antimony-based compounds. The digital photographs of metal precursor solutions (Fig. S1a), pristine Na metal (Fig. S1b), and Na anode modified with different antimony-based solution (Fig. S1c–e) in visually confirm the distinctions, and a formation of new layer over the Na metal. The in-situ reduction reaction was extremely fast, because of the lower electrochemical potential of Na metal than organic electrolyte.[15,33] and as soon as the solution was drop-casted, the color of the sodium surface immediately changed to yellowish ash from silvery white. To understand the structural composition of artificial SEI layer over Na metal anode, high-resolution 3D XRD was performed. The Na anode was chemically reduced by Sb_2S_3 solution, and the results are presented in (Fig. 1a). The XRD patterns indicate a formation of NaSbS complex majorly constituting Na_3SbS_4 phase over the Na metal. It is well known that Na_3SbS_4 is an excellent Na-ion conducting solid electrolyte with conductivity in the range of 10^{-3} to $10^{-4} \text{ s cm}^{-1}$ along with low activation energy, and several solution mediated synthesis of Na_3SbS_4 solid electrolyte was reported previously [34]. The XRD peaks indicates the highly crystalline nature of Na_3SbS_4 protective surface over Na metal. The ionic conducting SEI layer has a minor phase of Na_3Sb alloy, and inorganic Na_2S over modified metal anode. The presence of such mixed layer over metal anode can easily drive the sodium ion flux uniformly towards beneath the Na metal surface and make Na deposition beneath the protective layer efficiently [35]. Meanwhile, XRD pattern of other antimony alloy solutions treated Na metal showed different trend. In the NaSbI complex, the peaks at 29.03° and 42.13° correspond to Na metal (PDF: 22-0948), while another diffraction peak at 61.3° is characteristic of the Na_3Sb alloy (Fig. S2a). Additionally, a few peaks are indexed to the NaI phase as a by-product (PDF: 01-078-0602). Similarly, NaSbF complex has combination of Na_3Sb alloy and NaF phase over the Na metal surface (Fig. S2b). The presence of Na_3SbS_4 solid electrolyte is not observed in other alloys, and it is mainly due to thermodynamically favorable reactions between Na metal and the antimony alloy solution that drive the formation of solid electrolyte layer over Na metal with Sb_2S_3 solution. The thermodynamic energy required for formation of sodium antimony iodide/fluoride cannot be supplied by the chemical reduction of the precursor solution with Na metal. The Na_3Sb alloy layer possesses a low activation barrier and can facilitate a rapid diffusion of Na-ions across the interphase with low overpotential. The Na_2S byproduct is highly insulating and can make the hybrid artificial SEI layer highly resistive against electronic conductivity. The electrical field developing across these two phases can also provide a driving force for Na-ion diffusion through this layer, and induces Na plating underneath the hybrid artificial SEI layer [30,36].

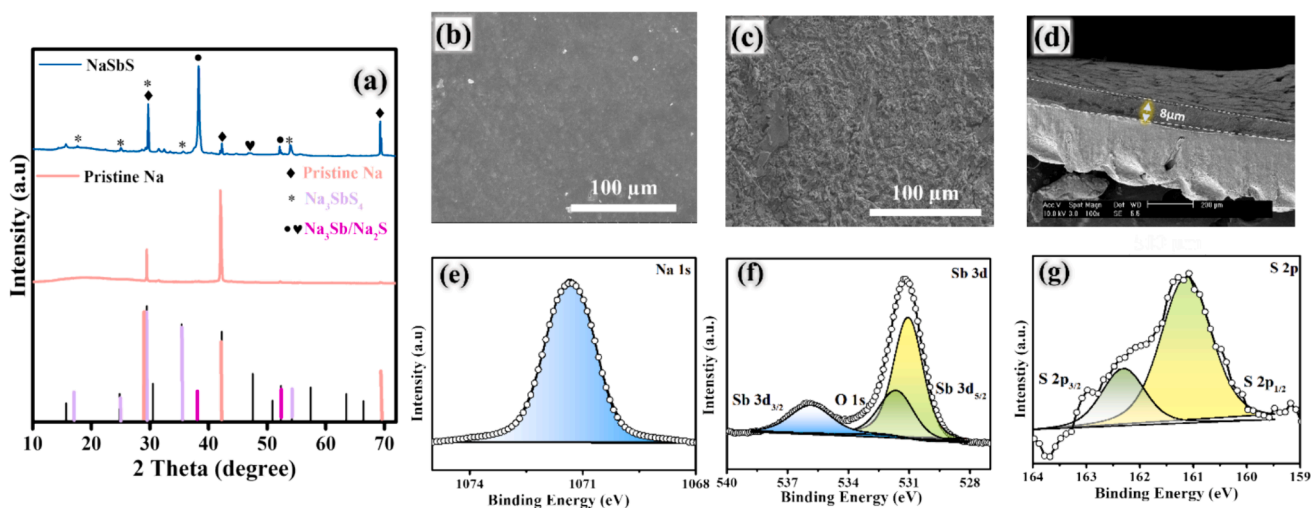


Fig. 1. a) XRD diffraction patterns of Na metal with NaSbS complex, b) SEM image of Na metal anode, c) SEM images of Na with NaSbS complex protective layer, d) Cross-sectional view of Na with protective layer, e–g) XPS spectra of Na metal with NaSbS complex SEI layer showing Na 1 s, Sb 3d, and S 2p spectrum

The morphological analysis of the pristine Na metal and Na metal anode with NaSbS complex were characterized using scanning electron microscopy (Fig. 1b,c). SEM images show that smooth and clear surface morphology for pristine Na, while the modified Na metal anode electrode was covered with a dense layer. This indicates a formation of new layer over the Na metal anode surface through the in-situ reduction [30]. The chemical interplay occurs between Na metal and antimony sulfide (Sb_2S_3) solution resulted in the formation of a highly well-embedded, dense, and thin protective layer over the Na metal anode. Cross-sectional SEM images (Fig. 1d) provided insights into the coating thickness, which was measured as 8 μm thin and uniform composition. The resulting interphase layer was chemically bonded with Na metal and, as formed protective layer is very thin and could increase the homogeneity to drive a sodium ion flux [37]. SEM images of the other antimony-based protected interfaces are presented in (Fig. S3a-c) and each of these electrodes showed different features owing to the different reduction potentials of the metal precursor solutions on the surface of Na metal. The protected electrode exhibited a distinct morphology that was attributed to the different reduction energy of the compounds with Na metal at room temperature.[38] The oxidation state and elemental composition of NaSbS complex over Na metal was examined using a vacuum-filled high-resolution X-ray photoelectron spectroscopy. The Na 1s spectrum is positioned at the binding energy of 1071 eV (Fig. 1e), indicating presence of Na-rich SEI layers over modified metal anode. The deconvoluted Sb 3d spectrum (Fig. 1f) at 531.01 eV for Sb 3d_{5/2} and 535.8 eV for Sb 3d_{3/2}, and the deconvoluted S 2p peaks (Fig. 1g) at 161.09 (S 2p_{1/2}) and 162.03 (S 2p_{3/2}) indicates the formation of Na_3SbS_4 type Na-ion conducting complex as artificial SEI layer over Na anode.[39].

3.1. Na deposition in pristine Na and Na anode with modified interface under high-current and high capacity

The Na deposition, and dendrite formation behavior in pristine Na metal anode and Na anode with modified interface was probed by depositing 2 mAh cm^{-2} of sodium ions at a current density of 2 mA cm^{-2} . The pristine Na electrode exhibited an irregular and rough surface, indicative of uneven sodium deposition and the formation of heterogenous natural SEI, as presented in (Fig. S4a). The heterogeneity of the pristine sodium electrode resulted in mossy Na deposits as the cycle increases and subsequent dendrite formation occurs.[40] In contrast, the surface of all modified metal anodes were highly uniform and smooth with no observable dendrites, as presented in (Fig. S4b-d). It is noted that the protective SEI layer restricts the direct contact of Na metal and electrolyte, which provided increased protection for sodium metal and ensured smooth electrochemical performance.[41] The cross-sectional SEM image of modified metal anode with NaSbS complex shows the Na deposition layer beneath the NaSbS complex (Fig. S5a,b). The high ionic conductivity of Na_3SbS_4 solid electrolyte as artificial SEI layer can easily drive the Na-ion flux uniformly towards beneath the SEI layer and make Na metal deposition beneath the protective layer efficiently. The difference in electronic conductivities of alloy phase and Na-rich inorganic phase also facilitated a rapid diffusion of Na-ion across the interphase with low overpotential [6]. The Energy dispersive spectroscopy (EDAX) mapping of modified Na anode (Fig. S5c-f) shows the uniform and denser distribution of Na, Sb, S elements on the surface, indicating the highly stable, and uniform nature of the NaSbS complex protective layer over the Na metal surface.[42] The modified Na anode with the NaSbS complex layer shows a smooth morphology without

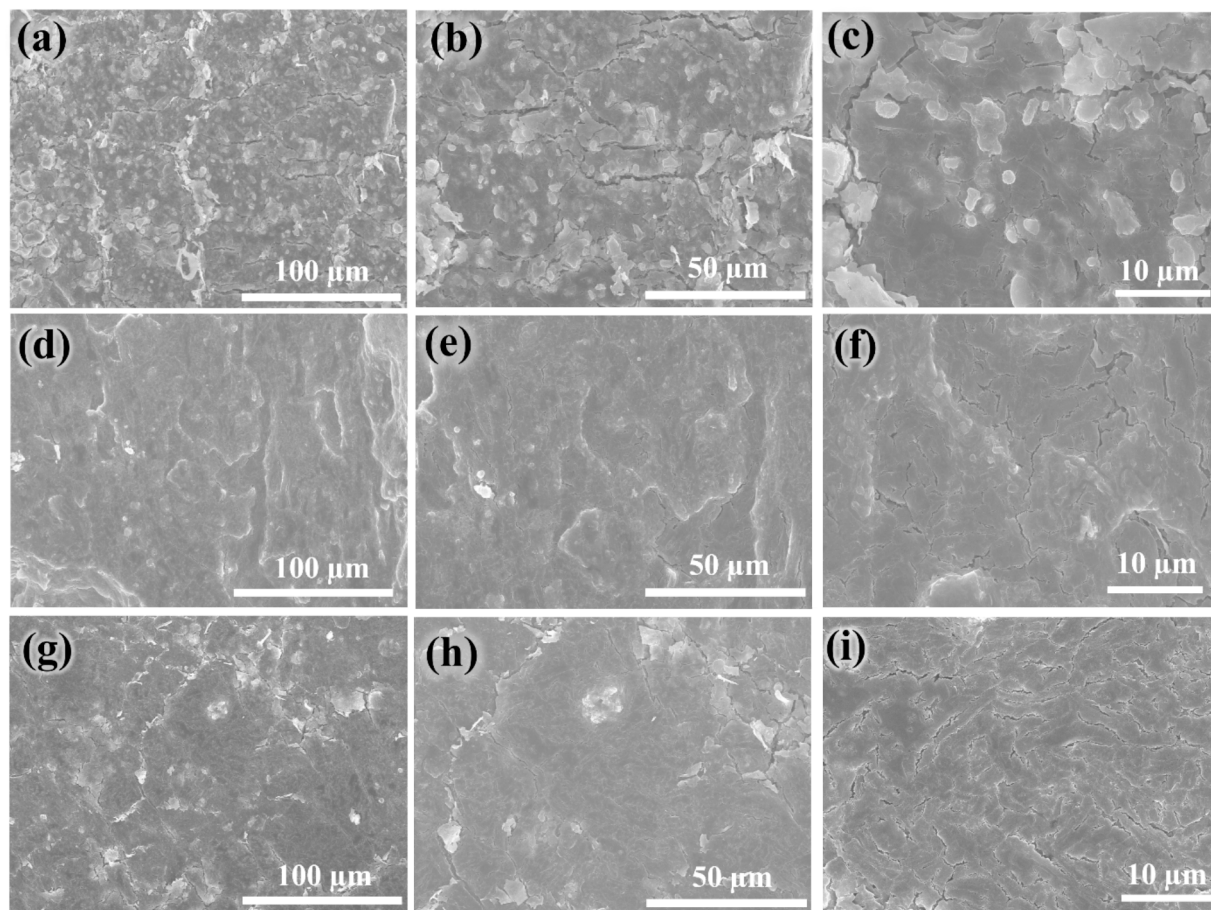


Fig. 2. Top-view SEM images of Na metal anode with NaSbS complex as artificial SEI layer at different Na deposited conditions: a-c) 2 mA cm^{-2} at 5 mAh cm^{-2} , d-f) 2 mA cm^{-2} at 10 mAh cm^{-2} g-i) 2 mA cm^{-2} at 30 mAh cm^{-2} .

dendrite formation and mossy deposits, even at higher Na deposition capacity of 5 mAh cm^{-2} (Fig. 2a-c). Furthermore, the modified metal anode can withstand a very high the areal capacity of 10 & 30 mAh cm^{-2} (Fig. 2d-i), without SEI layer rupture and dendrite formation, indicating a smooth distribution of sodium ion during plating and stripping. This was attributed to the high ionic conductivity of NaSbS complex layer, which allowed for a facile charge transfer and inhibited electron permeation. The artificial SEI layer not only prevented dendrite formation but also maintained the facile sodium plating and stripping for prolonged durations.[43] It should be noted that the Na metal anode with NaSbS complex layer can withstand such a huge volume change during 30 mAh cm^{-2} Na plating process even with a thinner artificial SEI layer, and it mainly attributed to high mechanical strength of the SEI layer. In comparison, the pristine Na metal anode exhibited considerable volume changes and a detrimental morphology with increasing sodium deposition (Fig. S6a-i). As the capacity increased to $5, 10$ and 30 mAh cm^{-2} under a fixed current density of 2 mA cm^{-2} , the resulting non-uniform and rough morphology is mainly attributed the formation of dense SEI layer by the unwanted side reactions during nucleation process.[44] The vertical growth of dendrites over pristine Na anode can also be noted and such high irregularity will maximize the local current density. The formation of vertical Na dendrites poses a significant risk, as they may puncture the separator, thereby potentially causing an internal short circuit.[42].

3.2. Plating/Stripping study of Na metal anodes

To gain a comprehensive understanding of the plating/stripping behavior on pristine Na metal and Na metal anode with artificially engineered interphase complexes, a long-term cycling study was

implemented with 1 h plating and stripping at a current density of 2 mA cm^{-2} and the results are presented in Fig. 3. 1 M NaPF_6 in diglyme electrolyte with a volume of $75 \mu\text{l}$ was used for this study. The voltage profiles in (Fig. 3a) unveiled distinct behaviors of each electrodes, where the pristine Na metal exhibited a high initial overpotential (20 mV), which was attributed to the naturally formed unstable SEI layer at the metal-electrolyte interface. Subsequently, the overpotential of the pristine Na metal increased to 60 mV , accompanied by a sudden voltage drop in 100 h . This signified the continuous occurrence of parasitic reactions leading to increased cell resistance between the interphases, which resulted in inevitable dendrite formation and cell failure.[42] By contrast, Na metal anode with NaSbS complex as artificial SEI layer interphase electrode delivered an impressive lifespan of over 1100 h along with minimal hysteresis potential (10 mV), and a stable voltage profile. The Na anode with NaSbS complex layer yielded superior performance owing to high conductivity and high interphase strength, which facilitates efficient sodium ion transport and minimized the volume-expansion related problems during repeated plating/stripping cycles.[45] Similarly, other modified anodes with NaSbI and NaSbF based complexes exhibits smooth and stable voltage behaviors over extended cycling periods than pristine Na metal with overpotential of 12 mV , and 14 mV respectively. The closer voltage profiles in a different time scale (Fig. 3b-e) the symmetrical cells shows that the Na metal with artificial interphase electrodes has smooth plating/stripping process than pristine Na electrodes. The hysteresis potentials of the Na anode with NaSbS, NaSbI, and NaSbF complexes remained low even after 100 cycles, at $13, 15$, and 16 mV respectively. By contrast, the pristine Na anode exhibited a drastic increase in hysteresis potential from 20 mV to 60 mV , which indicated uneven plating/stripping and high surface energy utilization for Na ion adsorption. However, the cycle life of other

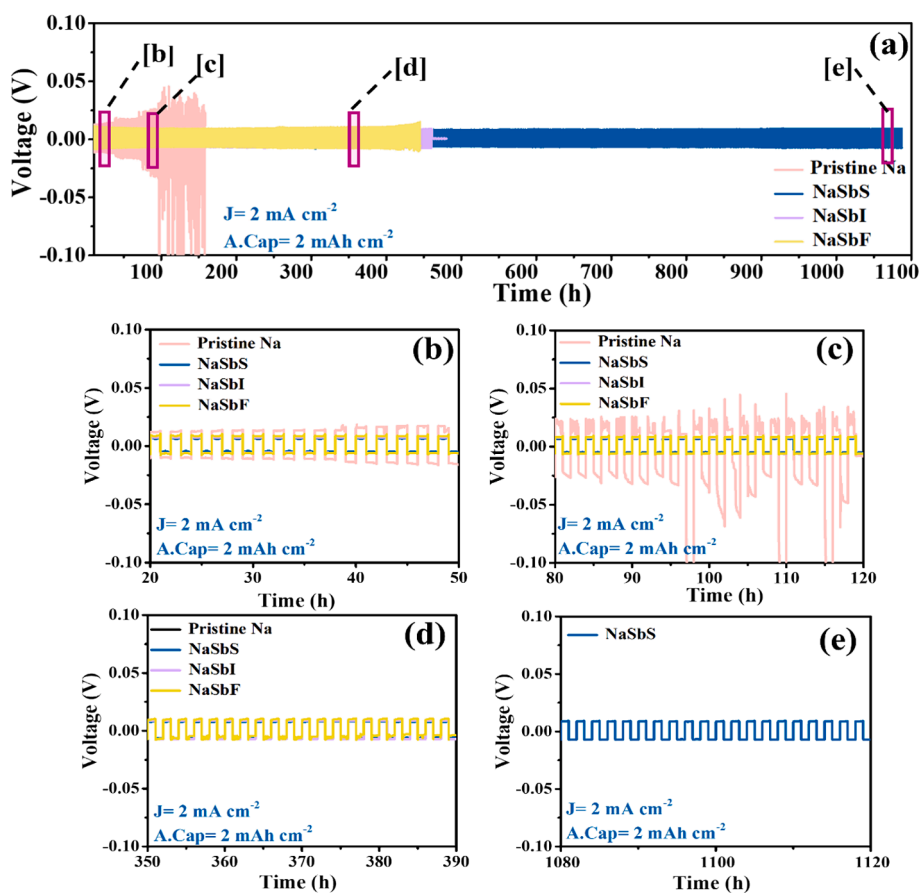


Fig. 3. Symmetric cell study of pristine Na electrode and modified anodes with different antimony interphases: a) Voltage vs. time profiles at 2 mA cm^{-2} and areal capacity of 2 mAh cm^{-2} , b-e) plating/stripping performances of each electrode in different time scales.

modified anodes without Na-ion conducting solid electrolyte (with only Na₃Sb alloy) is much lower lifespan than Na anode with NaSbS complex. The lower surface energies and diffusion barriers of Na-ion conducting NaSbS complex played a key role in faster Na adatom diffusion through the artificial SEI layer complexes, resulting in stable and efficient cycling performance.[46,47] The thickness of the NaSbS layer on the Na metal anode is controlled by varying the concentration of metal alloy solutions. To determine the optimal thickness, we tested electrodes using three different molar concentrations of Sb₂S₃ in tetrahydrofuran: 0.1 M, 0.15 M, and 0.25 M. These concentrations represent low, medium, and high thickness, which influence the electrochemical properties of the Na metal anode with artificial SEI layers. For each variation, analyzed the morphology, cycling stability, and impedance spectroscopy at low current density and areal capacity. These analyses helped us to understand the impact of thickness on electrochemical performance and identify optimal conditions for achieving superior performance. At a 0.1 M concentration, the as-formed SEI layer is likely thinner and less dense, providing low effective protection to the electrode surface (Fig. S7a,b). At a 0.15 M concentration, the as-formed SEI layers exhibit a smooth and uniform morphology with optimal thickness. This layer is neither too thick nor too thin, allowing for uniform sodium ion transport. This optimal thickness contributes to long-term cycling stability with lower overpotential (Fig. S7c,d). At a higher 0.25 M concentration, the SEI layers appear very tight and thick due to the high concentration. The increased thickness results in higher impedance because the thicker layers create an energy barrier, restricting the easy flow of sodium ions into the structure (Fig. S7e,f). After analyzing their morphology, symmetric cell performance was conducted to study the plating/stripping performance. Both low (0.1 M) and high (0.25 M) concentrations result in high nucleation overpotential and non-uniform sodium ion plating/stripping, leading to poor cycling stability. In contrast, the NaSbS anode with a 0.15 M concentration provides optimal thickness, ensuring non-dendritic sodium ion deposition and a flat overpotential over prolonged cycling compared to other variations. (Fig. S8a). Very low or high thickness creates a less stable interphase layer between the metal and anode, significantly influencing interphase properties. When treated with a low concentration of metal alloy solution, the sodium metal anode forms a thin and incomplete SEI layer. At high concentrations (0.25 M), the SEI layer becomes rough and thick, resulting in higher interphase resistance that slows sodium ion diffusion. Additionally, performed the impedance analysis after 50 cycles, to look at how the thickness of the SEI layer affects resistance (Fig. S8b). The Nyquist plots show that the NaSbS anodes at 0.15 M have lower interface resistance than those at 0.1 M and 0.25 M. This is due to the SEI layer at 0.15 M having the optimum thickness and interfacial strength, which helps to reduce unwanted electron transfer and improves overall battery performance. Moreover, a comparative analysis showed that the antimony-

based artificial SEI complexes developed in this work outperformed the previous reports, emphasizing the effectiveness of the proposed approach (Supporting information Table S1). A comprehensive schematic outlining the fabrication process and chemical interactions of the ionically conducting protective layer is given in (Fig. 4a&b). The scheme highlights the interfacial changes that occurred in both pristine Na and Na metal with Na-ion conducting solid electrode complex as artificial SEI layer. The newly formed interface has high ionic conductivity and robust, resulting in uniform plating/stripping. By contrast, the pristine Na exhibited uneven sodium ion deposition due to naturally formed non-uniform SEI layer.[9,48]. This non-uniformity continues throughout the plating/stripping process, causing the volume of the sodium metal to expand and contract simultaneously. Eventually, these soft dendrites can evolve into needle-shaped structures that grow towards the opposite electrode. The antimony-based Na ion conducting complex as the protective layers on Na metal formed by facile chemical reduction approach can undergo multiple plating/stripping cycles without dendrite formation.

3.3. SEI layer chemical composition and stability

It is important to validate the structure and integrated components of the SEI layers, which are directly linked to dendrite growth formation, by using high-vacuum X-ray photoelectron spectroscopy. XPS analysis was carried after 100 plating/stripping cycles on Na metal anode with NaSbS complex as artificial SEI and the results are presented in Fig. 5. The primary focus was on the Na 1s, Sb 3d, and S 2p as they constitute major components of the artificial SEI layer. The Na 1s spectrum at 1071 eV (Fig. 5a) gives the contributions from several Na rich inorganic SEI phases like Na₂S, NaF, and NaSbS. The Sb 3d spectrum exhibited two distinct peaks at 526.6 eV (Sb 3d_{5/2}) and 539.3 eV (Sb 3d_{3/2}), as presented in (Fig. 5b), originating from NaSbS phase and NaSb alloy of SEI layer. An oxidized antimony peak which overlapped at 534 eV, suggested surface oxidation reactions of the electrodes with the atmosphere occurred during the sample handling process. The S 2p located at 162.2 eV indicated chemical interaction between sodium and sulfide (Na-S) on the surface, as presented in (Fig. 5c). The above XPS results confirms the robust stability of the artificial interphase layers which also persisted even after numerous plating/stripping cycles.[49] After 100 cycles, additional elements such as P 2p and F 1s were also observed, signifying the formation of NaP, and C-F, Na-F, possibly owing to interactions between the organic electrolyte components and protected metal alloys on the surface due to the electrolyte decomposition during initial cycles, as presented in (Fig. 5d,e). The C 1s spectrum deconvoluted into peaks at 284.59, 285.4, and 288.6 eV representing the O-C=O, C-O-C, C-C functional groups, respectively (Fig. 5f), and the XPS results further emphasized the stability of the SEI layer after continuous cycling. The

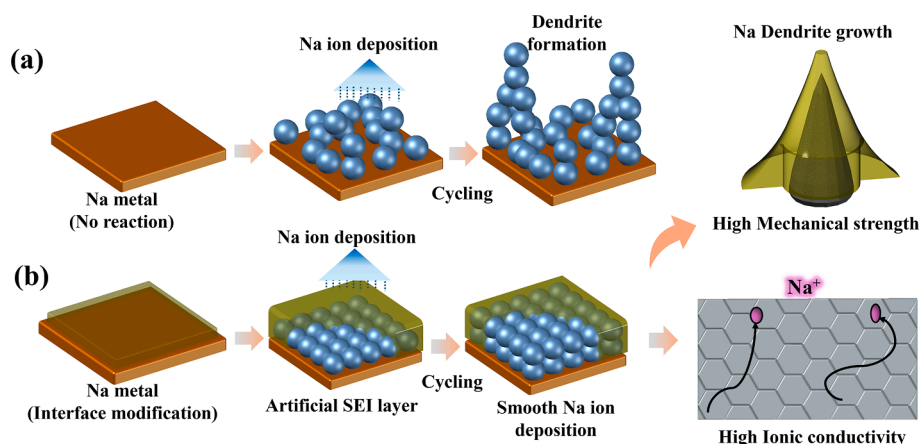


Fig. 4. Schematic illustration, fabrication process, and cycling process of electrodes with a) Pristine Na and b) Artificial-interphase layers.

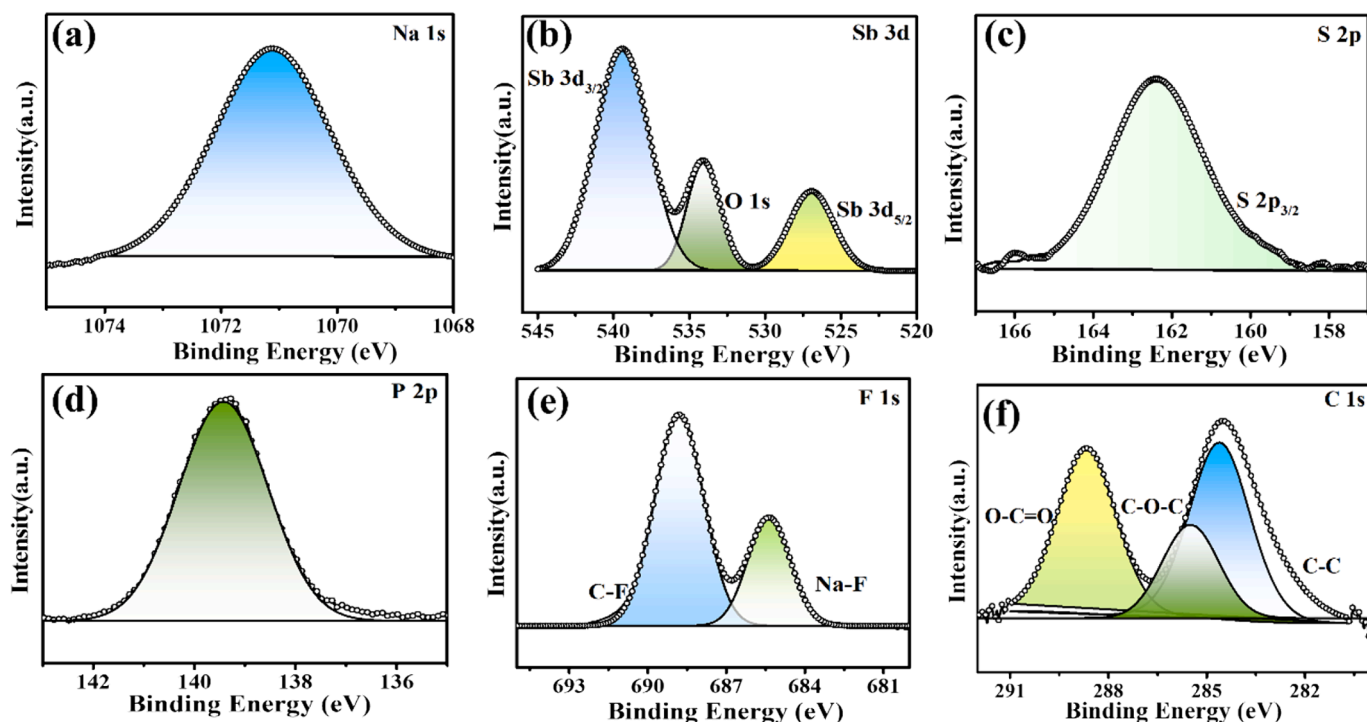


Fig. 5. High-resolution XPS spectrum after 100 cycles of plating/stripping, Na metal anodes with NaSbS complex as SEI layer: a) Na 1 s, b) Sb 3d, c) S 2p, d) P 2p, e) F 1 s, and f) C 1 s.

consistent spectrum suggested that the isolated SEI layer is remained stable, and it was minimally affected by side reactions.[50] The XPS results of Na metal anode with NaSbI and NaSbF complexes as artificial SEI layers were also measured after 100 cycles and results are presented in (Fig. S9 a–f). The results show a similar trend on physical stability of artificial SEI layer formed over the Na metal anode.

3.4. Na Plating/Stripping behavior at higher rates

The electrochemical performance was systematically studied under high capacity and current density condition to understand the reaction kinetics of the pristine Na metal anode and the modified anodes. In symmetric cell testing, at a Na deposition capacity of 5 mAh cm^{-2} and 2 mA cm^{-2} current density, the pristine Na electrode exhibited a stable life up to 100 h and a substantial overpotential of 50 mV, (Fig. 6a) owing to large volume changes of Na metal at high capacity Na deposition conditions.[51] However, the Na metal anode with NaSbS artificial layer delivered a remarkably stable plating/stripping profile over 872 h with an overpotential of less than 15 mV. The artificial SEI layer makes the Na metal anode mechanically stable and exhibited a smooth interface, which enhanced the Na^+ diffusion rate and stabilizing the interface even at high Na deposition.[16] To further assess the reaction kinetics at higher rates, the areal capacity was increased to 10 mAh cm^{-2} , while maintaining the current density at 2 mA cm^{-2} . The modified Na metal anode exhibited an extended lifespan of around 835 h with a low potential of 20 mV (Fig. 6b). The higher stability and higher efficiency of the modified anode are mainly due to low impedance resistance exhibited at electrode–electrolyte interface, after formation of artificial SEI layer. By contrast, the pristine Na anode exhibited uneven capacity from the initial cycle, leading to uneven and unsmooth plating on the surface. Subsequently, owing to uneven deposition on the Na anode, and continuous rupture and formation of new SEI layer, the overpotential of pristine Na was increasing continuously. When the areal capacity was increased to 30 mAh cm^{-2} at the current density of 2 mA cm^{-2} , as presented in (Fig. 6c), the pristine Na electrode yielded an extremely high overpotential of 60 mV from the outset of the nucleation process,

exhibiting non-uniform plating/stripping along with poor coulombic efficiency. During high areal capacity utilization, the host less nature of the Na metal anode will experience huge volume expansion and contraction. However, the natural solid electrolyte interface (SEI) layer does not respond immediately to high pressure; instead, it generates stress during the initial nucleation process. This stress ultimately contributes to the repair of the SEI layer, reducing the stability and longevity of the anode.[52] The increase in overpotential at high Na deposition was mainly ascribed to the structural damage of the naturally formed SEI layers that cannot withstand high pressure and high Na deposition load. However, The modified Na metal anode with Na-ion conducting NaSbS complex SEI layer accommodated a larger amount of sodium ions (30 mAh cm^{-2}) smoothly [16,52,53] even after many cycles, indicating the robust nature of the SEI layer. It exhibited uniform plating/stripping behavior over an extended duration of $> 800 \text{ h}$ while maintaining consistent and ultra-low hysteresis ($< 20 \text{ mV}$). During high amount of Na ion deposition, the Na-ion migration energy on the modified anodes is lower due to presence of Na-ion conducting solid electrolyte as artificial SEI which also has high mechanical strength, thus improving the long-term cyclic stability. It should be noted that, even at the high areal capacity of 30 mAh cm^{-2} , the studied artificial SEI layers outperformed several previous works (Supporting information Table S2), and it is the highest capacity reported to date with high cycle life. Similarly, the Na metal anode with other artificial SEI layers shows better performance than pristine Na metal (Fig. S10–S12), but lower cycle life than NaSbS complex. The rate performance of Na metal anode with NaSbS complexes were also tested at different capacity (sequential increase 2 to 30 mAh cm^{-2}) and current rates (sequential increase from 2 mA cm^{-2} to 10 mA cm^{-2}), and the modified electrode exhibited remarkable stability and uniform behavior, due to the highly stable artificial SEI layer, showcasing its adaptability across varying conditions. Even when subjected to significant current and volume variations, the Na anode with NaSbS artificial layer remained stable and robust due to benefits from artificial SEI layer. In contrast, the pristine Na electrode displayed high voltage hysteresis, owing to the unexpected current and capacity changes during plating and stripping process. The abrupt

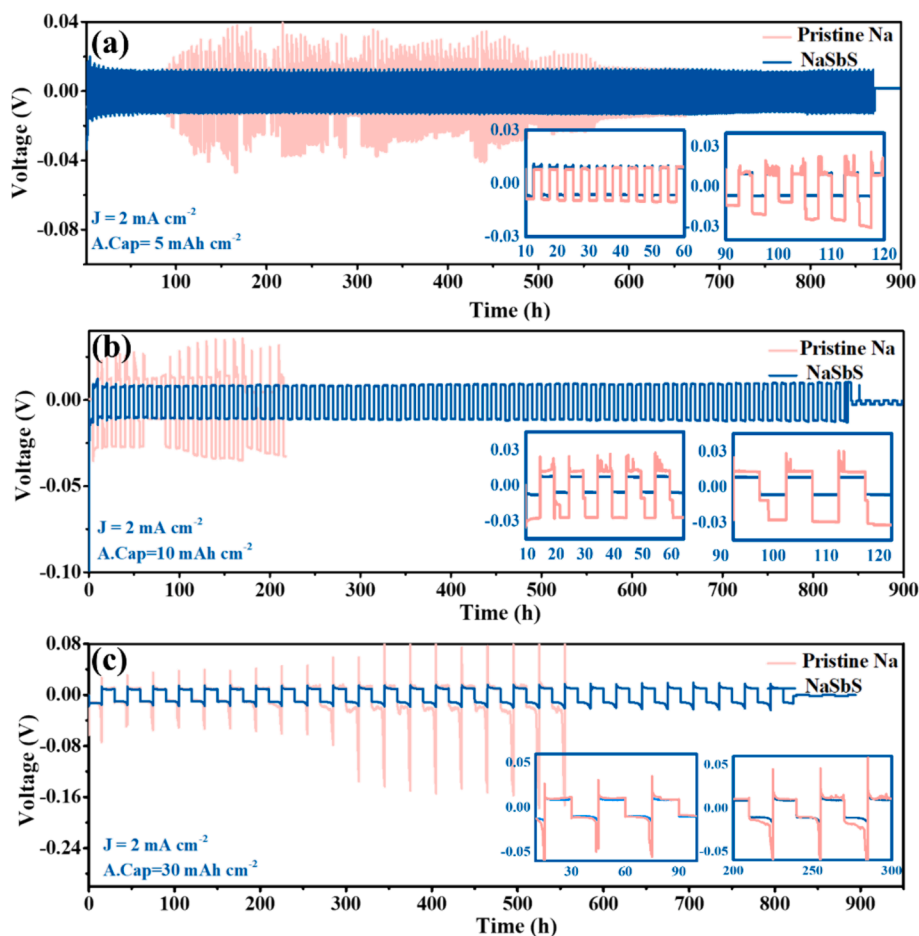


Fig. 6. Symmetrical cell study of pristine Na and modified anode with NaSbS complex artificial SEI layer at different conditions: a) 2 mA cm^{-2} & 5 mAh cm^{-2} , b) 2 mA cm^{-2} & 10 mAh cm^{-2} , c) 2 mA cm^{-2} & 30 mAh cm^{-2} .

tolerance limits of naturally formed SEI layer to capacity and volume changes are very low while Na anode with artificial SEI layer can withstand vigorous volume from (2 to 30 mAh cm^{-2}) under rapid variations. Na anode with NaSbS complex demonstrated sustained stability, even when the current density increased abruptly due to the high mechanical strength and the cell maintained stable capacity. Conversely, when the pristine Na metal was subjected to a continuous increase in current density, it succumbed to these changes primarily because of its low interface strength. (Fig. S13 a,b).

To assess the mechanical strength of the Na metal anode with NaSbS complex protective layer, AFM was employed. Initially, prior to the electrodeposition of Na, AFM studies were conducted on pristine Na metal anode, and Na metal anode with NaSbS complex as artificial SEI layer. The average Young's modulus value of modified metal anode was determined to be 8.539 GPa , with a standard deviation of 2.932 GPa (Fig. 7a). The young's modulus difference is accordance with the strength of the artificially coated SEI components on the surface of pristine Na metal.[5,8] In contrast, for pristine Na, the average Young's modulus value is 2.261 GPa , and the standard deviation of 1.726 GPa . It should be noted that the mechanical strength of the Na metal anodes with solid electrolyte complex as artificial SEI layer has much higher stability than Na anode with alloy type artificial SEI layer.[5,54,55] Furthermore, the mechanical strength of the pristine Na metal and modified Na metal after Na deposition were also evaluated using AFM technique. Initially, 5 and 30 mAh cm^{-2} capacity of Na ions were directly electrodeposited on both Na and metal anode with multifunctional NaSbS interphase. At 5 mAh cm^{-2} Na deposition, the average Young's modulus value of modified metal anode is 8.292 GPa and the

standard deviation of 3.109 GPa (Fig. 7b), which is 4 times higher than that of pristine Na (2.307 GPa , with a standard value of 1.34 GPa). Under the 30 mAh cm^{-2} electrodeposited conditions, the average Young's modulus value of Na-SbS is 8.303 GPa , a standard deviation of 2.738 GPa (Fig. 7c), which is higher than that of pristine Na (2.170 GPa , with a standard value of 1.533 GPa). The observed Young's modulus value of Na anode with NaSbS complex shows similar values even after large volume of Na deposition process. However, the mechanical stability of the SSE based NaSbS protective layer is not affected by increasing the areal capacity to 5 and 30 mAh cm^{-2} . This robustness effectively restricts dendrite formation on the surface. Similarly, the Young's modulus distribution of pristine Na and electrodeposited pristine Na also exhibits similar values, but it is prone to the separator due to the inhomogeneous distribution, leading to a short circuit [56].

The hybrid interphase over the Na metal was further studied by impedance spectroscopy. The impedance spectroscopy can provide new insights into the diffusion mechanisms within the hybrid interphase layers. The Nyquist plots of symmetric containing pristine Na metal anode and modified metal anodes are measured before cycling and after cycling, and the results are presented in (Fig. S14 a,b). Before cycling, the pristine Na anode and modified Na metal anode showed a semicircle in the high-frequency region (indicative of interphase layer resistance) owing to the formation of artificial and natural SEI interphases, while the semicircles in the low-frequency region represented the total charge transfer resistance between the electrodes and the electrolyte. The interfacial resistance of the pristine Na electrode was lower before cycling but increased significantly after 200 h of cycling (100 cycles). This was attributed primarily to the instability of the naturally formed

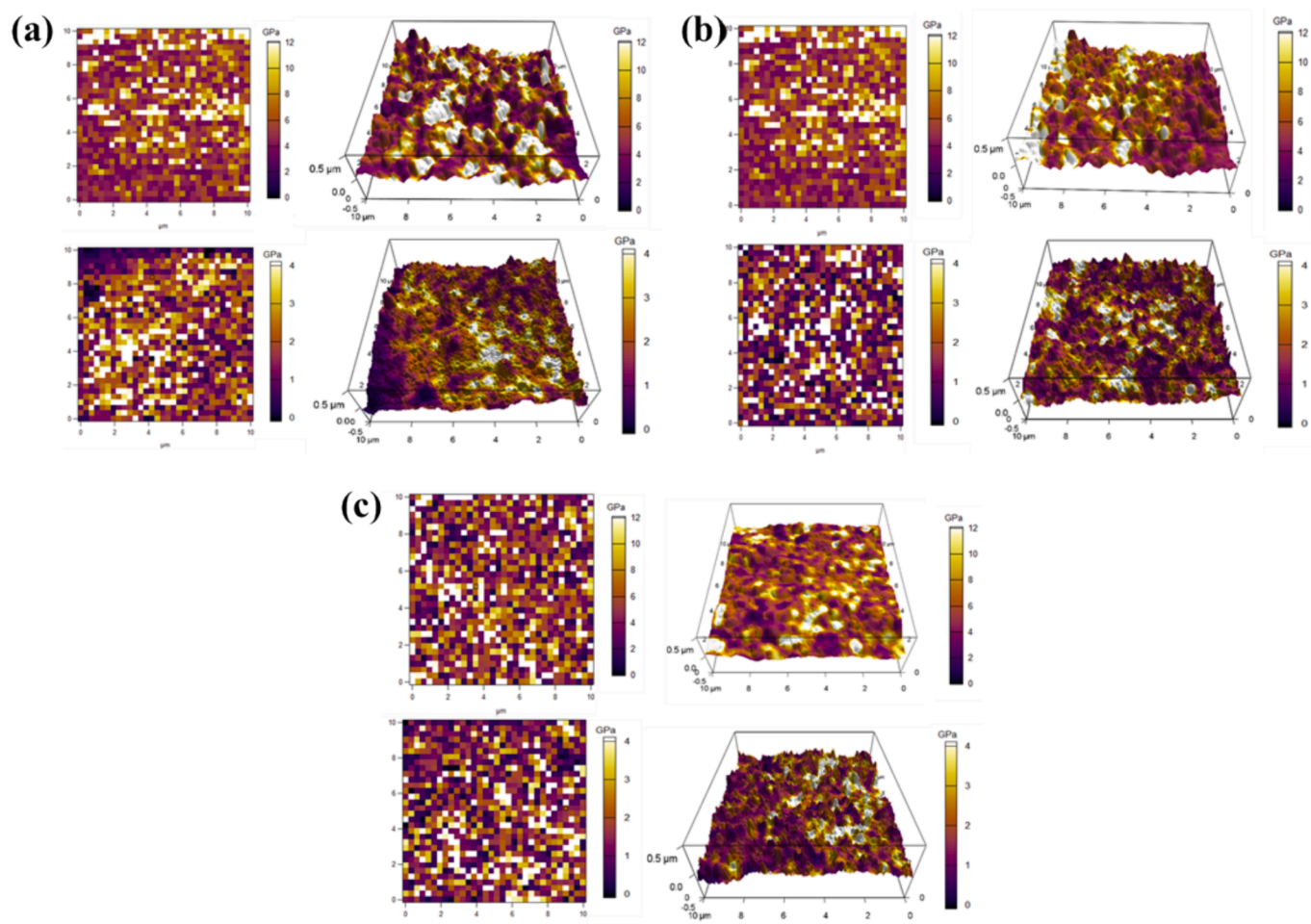


Fig. 7. Young's modulus distribution of Pristine Na metal (bottom), and Na metal with NaSbS complex as SEI layer (top) at different conditions, (a) before Na deposition, (b) 5 mAh cm^{-2} of Na deposited at 2 mA cm^{-2} , and (c) 30 mAh cm^{-2} of Na deposited at 2 mA cm^{-2} .

SEI heterogeneous layer after prolonged cycling, and the resulting high charge transfer resistance impeded the diffusion of Na ions into the structure.[57] The periodic consumption of electrolyte for repeated SEI layer formation will greatly increase the internal resistance of the cell with pristine Na metal. The Na anode with artificial SEI layer initially showed higher resistance than naturally formed SEI layers due to higher impedance resistance contribution from the extra artificial layer. However, during continuous plating/stripping, the artificially formed SEI layer became well embedded with natural SEI layer, leading to a decrease in resistance.[58] The charge transfer resistance of the Na metal anode with artificial SEI layer has significantly reduced, suggesting the improved charge transfer kinetics and super-fast diffusion at the interface after modification. The lower the charge transfer resistance, the easier is the facilitation of Na ions near the anode for nucleation. Therefore, artificial SEI protective layer with minimal interfacial resistance holds promise for designing high-energy-density rechargeable batteries.[59] A comparative microstructural analysis on Na metal anode and modified Na metal anode after cycling process (100 cycles at 2 mA cm^{-2} & 2 mAh cm^{-2}) were studied using SEM, and the results are given in (Figs. S15 a-i). A noticeable variation on the surface of pristine Na metal anode, and Na metal anode with protective SEI layer can be clearly observed after cycling. The surface of modified Na metal anode exhibited extremely smooth and uniform morphologies without any cracks even after 100 plating/stripping cycles. The as formed artificial interphase has high potential to reduce the unwanted side reactions, thus helping to maintain the smooth surface without dendrite formation. In contrast, the pristine Na metal anode exhibited a heterogeneous

surface with uneven nucleation with numerous stacked sheet-like morphology. The uneven sodium ion flux was generated and continuous SEI layer rupture/regeneration results in active dendrite growth over Na metal anode.[4] Furthermore to discover the novelty of the proposed method, after several cycles of plating/stripping, those cycled electrodes of pristine Na and NaSbS electrodes underwent and detailed study. We measured the impedance of the electrodes and studied their surface interface resistance to evaluate the superior cycle life performance of the robust artificial SEI-based electrodes. The interfacial resistance of the pristine Na before cycle is 7Ω , due to the natural SEI layer formation (Fig. S16a). Afterwards, when the cycle increases to 150, 200 and 250th, the resistance also gradually increases to 24.61Ω , 43.33Ω and 93.95Ω respectively. The trend in increasing resistance is mainly due to the fragility of the natural solid electrolyte interphase layer, which leads to the continuous uneven sodium ion deposition with high impedance resistance and dendrite formation. In contrast, before cycling NaSbS electrode shows the high impedance resistance of 24.46Ω , which is mainly ascribed to the insulating property (Fig. S16b). After that, their resistance got stabilized well with the continuous plating/stripping, which is well related with the interphase strength of the sodium ion conducting NaSbS electrodes, respectively. Further support the interfacial resistance of the pristine Na and NaSbS electrodes, their surface morphology studies were conducted. Before taking to the SEM analysis, cells were broken, and electrodes washed with tetrahydrofuran solvent to remove the impurities. Even after encountering many cycles as 150, 200 and 250th, the NaSbS electrode shows the compact, dense and smooth morphology rather than the sodium dendrites which could

be the reason for long term cycle performance (Fig. S17a-i). To further evidence dendrite formation, we subjected pristine sodium metal anodes to various cycles at 2 mA cm^{-2} and 2 mAh cm^{-2} areal capacity. After 150, 200, 250, and 300 cycles of plating/stripping on pristine Na, the cells were dismantled, and their morphology was analyzed using SEM (Fig. S18, S19). Upon closer examination, small dendrites were observed, growing in a dispersive manner. Over time, specific spots tended to develop into sharp structures that could potentially penetrate the separator (Fig. S18a-i). Different magnifications were used to observe the non-uniformity that occurs during continuous cycling. In (Fig. S19 a,b) After 300 cycles both surface and cross-sectional SEM images reveal aggressive dendrite formation, primarily due to the highly loose, naturally formed solid electrolyte interphase (SEI) layer. A heterogeneous SEI layer promotes non-uniform sodium ion transportation, leading to structural collapse and needle-like growths that can penetrate the separator.

3.5. Full cell and Solid-State battery

A full cell using Na anode with/without NaSbS complex layer coupled with a high voltage $\text{Na}_{1.2}\text{Mn}_{0.8}\text{O}_{1.5}\text{F}_{0.5}$ cathode (NMF), was assembled, schematic shown (Fig. 8a). The pristine Na || NMF cell exhibited discharge capacities of 160, 146, 130, and 120 mAh g^{-1} respectively when the current rates were increased from 0.1C, 0.2C, 0.5C and 1C (Fig. 8b). In comparison, Na-NaSbS || NMF cell exhibited discharge capacities of 164, 150, 138 and 125 mAh g^{-1} , respectively at the 0.1C, 0.2C, 0.5C and 1C (Fig. 8c). The rate performance in Fig. 8d shows that the Na-NaSbS || NMF cell delivered higher capacity than

pristine Na cell at higher current rate due to enhanced Na-ion diffusion kinetics with modified artificial SEI. The capacity and coulombic efficiency of the cells with pristine Na metal anode drastically reduces after 50 cycles ($<40\%$) but the Na-NaSbS || NMF cell underwent an efficient cycling for 100 cycles with $>99\%$ coulombic efficiency even at 1C. This was attributed to the NaSbS complex protective layer, which effectively controlled dendrite formation on the anode side while ensuring high specific capacity and robust cycle stability. In contrast, the pristine Na anode showed poor performance primarily owing to the unstable SEI layer (Fig. 8e). The superior rate performance and cycling behavior of the NaSbS || NMF cells shows promising results for development of a highly attractive device for next-generation batteries. In the pursuit of practical applications of sodium metal anodes in all solid-state sodium batteries, we meticulously assembled symmetric cells by utilizing Na anode with NaSbS complex as artificial SEI layers as the electrodes and Na_3SbS_4 as the solid-state electrolyte, as illustrated in (Fig. 8f). In ASSBs, the electrolyte often poses challenges due to poor physical contact with the interfaces, poor chemical/electrochemical/thermodynamical instability of the metal anode. The Na metal anodes with artificial SEI layers are known to have favorable interface stability against the solid electrolyte. The pristine Na symmetric cell exhibited a continuous instability upon cycling as noted from increase in overpotential with time during Na ion deposition/stripping process.[50] This increase was mainly attributed to uneven Na metal-solid electrolyte interface, resulting in unavoidable side reactions. The side reactions lead to formation of several unwanted poor Na-ion conducting products, hindering the facile Na-ion conduction between the Na anode and solid electrolyte. The elevated interface resistance contributed to increased overpotential,

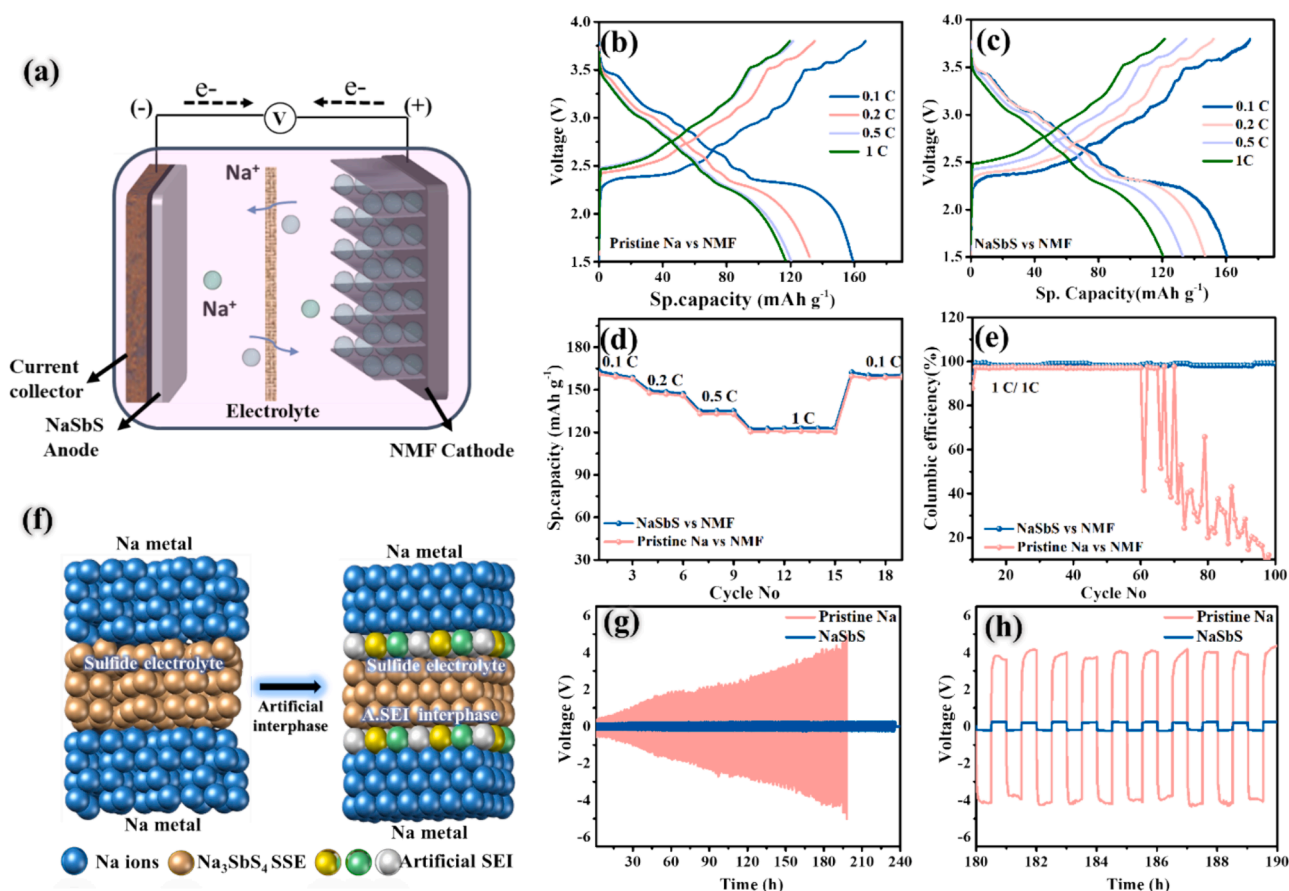


Fig. 8. Full cell Testing of Na-NaSbS anode vs. NMF cathode: a) Schematic illustration of charge/discharge mechanism in sodium metal battery, b) charge/discharge profile of pristine Na vs. NMF cathode c) Charge/discharge profile of Na-NaSbS anode vs NMF cathode. d) Rate performance and e) cycling stability at 1C; Electrochemical performance of sodium solid-state batteries: f) Scheme on solid state symmetrical cell, and g&h) Symmetric cell performance, Voltage vs. time profile at 0.05 mA cm^{-2} , 60°C .

which restricted the diffusion of Na ions.[60]. Furthermore, the capacity decay of the pristine Na cell, verified by dismantling the cell after 30 cycles of plating/stripping, the pristine Na metal anode and the Na₃SbS₄ SSE pellet, respectively. Dendrite formation occurs on the sodium metal surface (Fig. S20 a,b), where large nucleation potential and poor interfacial contact occurs, resulting in high impedance between the metal and electrolyte. The morphology appears loose and damaged due to dendrite formation. These dendrites can penetrate the Na₃SbS₄ pellet and induce the cracks in it.[61,62] In sharp contrast, the Na-NaSbS || Na₃SbS₄ || NaSbS-Na cell presented a flat, even, and smooth voltage profile for > 235 h at a current density of 0.05 mA cm⁻² and 30-min continuous charge/discharge cycle at 60 °C(Fig. 8 g&h). The artificial SEI provides a chemically favorable interface for the facile Na-ion conduction between the electrodes through the solid electrolyte. The result highlighted the enhanced performance and excellent interface stability of the Na anode with artificial SEI even in conjunction with the solid-state electrolyte, thus demonstrating its potential for integration with all solid-state sodium batteries..

4. Conclusion

In summary, we have thoroughly explored the characteristics of several Na-ion conducting antimony based solid electrolyte complexes as artificial SEI layers acting as protective coatings for non-dendritic sodium metal anodes. The thin artificial SEI layers made by simple chemical reduction reaction exhibited an impressive feature of high ionic conductivity and substantial mechanical properties. The protective layer not only ensured a consistent and uniform Na metal deposition at the strengthened interfaces but also effectively hindered electron tunneling from the Na metal anode. Na metal anode with NaSbS complex as artificial SEI layer exhibited remarkable stability over 1100 h with minimal overpotential, addressing the challenges associated with dendrite formation. The mechanical strength of the solid electrolyte type artificial SEI layers are higher than conventional inorganic, organic and alloy type SEI, helping to efficiently drive large deposition (30 mAh cm⁻²) and withstand > 800 h of cycling. Moreover, the hybrid SEI provides excellent flexibility to accommodate the huge volume changes occur during the Na deposition and can efficiently regulate the Na⁺ ion flux at high current density (10 mA cm⁻²) by reducing the local current density. The modified anode when couple with high voltage NMF cathode, and sulfide based solid electrolyte, exhibited excellent interface stability, coulombic efficiency, and long-term cyclic stability. Our findings are very significant in that it provides a straightforward approach for developing diverse applications using high energy sodium metal batteries and solid-state sodium batteries.

CRedit authorship contribution statement

Megala Moorthy: Writing – original draft, Methodology, Investigation, Formal analysis, Data curation, Conceptualization. **Ranjith Thangavel:** Writing – review & editing, Supervision, Investigation, Formal analysis, Data curation, Conceptualization. **Bala Krishnan Ganesan:** Investigation, Formal analysis, Data curation. **Aditi Saha:** Validation, Investigation, Formal analysis. **Seungbum Hong:** Validation, Supervision, Investigation, Formal analysis. **Yun-Sung Lee:** Writing – review & editing, Supervision, Software, Resources, Project administration, Investigation, Funding acquisition, Formal analysis.

Declaration of competing interest

The authors declare that they have no known competing financial interests or personal relationships that could have appeared to influence the work reported in this paper.

Data availability

Data will be made available on request.

Acknowledgements

This work was financially supported by a National Research Foundation of Korea (NRF) grant funded by the Korean government (Ministry of Science, ICT & Future Planning) (No. RS-2023-00208361). Dr. Ranjith Thangavel acknowledges the support from the Ministry of Earth Sciences, Government of India under the Deep Ocean Mission scheme (MoES/PAMC/DOM/03/2022).

Appendix A. Supplementary data

Supplementary data to this article can be found online at <https://doi.org/10.1016/j.cej.2024.155234>.

References

- [1] B. Moorthy, J.H. Kim, H.W. Lee, D.K. Kim, Vertically aligned carbon nanotubular structure for guiding uniform lithium deposition via capillary pressure as stable metallic lithium anodes, *Energy Storage Mater.* 24 (2020) 602–609, <https://doi.org/10.1016/j.ensm.2019.06.016>.
- [2] X. Zheng, H. Fu, C. Hu, H. Xu, Y. Huang, J. Wen, H. Sun, W. Luo, Y. Huang, Toward a stable sodium metal anode in carbonate electrolyte: a compact, inorganic alloy interface, *J. Phys. Chem. Lett.* 10 (2019) 707–714, <https://doi.org/10.1021/acs.jpcclett.8b03536>.
- [3] B. Moorthy, S. Kwon, J.H. Kim, P. Ragupathy, H.M. Lee, D.K. Kim, Tin sulfide modified separator as an efficient polysulfide trapper for stable cycling performance in Li-S batteries, *Nanoscale Horizons*. 4 (2019) 214–222, <https://doi.org/10.1039/c8nh00172c>.
- [4] Y. Gu, W.W. Wang, Y.J. Li, Q.H. Wu, S. Tang, J.W. Yan, M. Sen Zheng, D.Y. Wu, C. H. Fan, W.Q. Hu, Z. Bin Chen, Y. Fang, Q.H. Zhang, Q.F. Dong, B.W. Mao, Designable ultra-smooth ultra-thin solid-electrolyte interphases of three alkali metal anodes, *Nat. Commun.* 9 (2018), <https://doi.org/10.1038/s41467-018-03466-8>.
- [5] P. Shi, S. Zhang, G. Lu, L. Wang, Y. Jiang, F. Liu, Y. Yao, H. Yang, M. Ma, S. Ye, X. Tao, Y. Feng, X. Wu, X. Rui, Y. Yu, Red phosphorous-derived protective layers with high ionic conductivity and mechanical strength on dendrite-free sodium and potassium metal anodes, *Adv. Energy Mater.* 11 (2021) 1–10, <https://doi.org/10.1002/aenm.202003381>.
- [6] Y. Zhao, K.R. Adair, X. Sun, Recent developments and insights into the understanding of Na metal anodes for Na-metal batteries, *Energy Environ. Sci.* 11 (2018) 2673–2695, <https://doi.org/10.1039/c8ee01373j>.
- [7] S.J. Lee, M. Moorthy, S. Park, Y.S. Lee, Enhanced nitrogen-doped reduced graphene oxide-embedded MnMoO₄ as high-capacity and stable anode for sodium-ion batteries, *J. Ind. Eng. Chem.* 131 (2024) 199–207, <https://doi.org/10.1016/j.jiec.2023.10.019>.
- [8] Y. Zhao, L.V. Goncharova, A. Lushington, Q. Sun, H. Yadegari, B. Wang, W. Xiao, R. Li, X. Sun, Superior stable and long life sodium metal anodes achieved by atomic layer deposition, *Adv. Mater.* 29 (2017) 1606663, <https://doi.org/10.1002/adma.201606663>.
- [9] X. Wang, J. Lu, Y. Wu, W. Zheng, H. Zhang, T. Bai, H. Liu, D. Li, L. Ci, Building stable anodes for high-rate na-metal batteries, *Adv. Mater.* 2311256 (36) (2024) 2311256, <https://doi.org/10.1002/adma.202311256>.
- [10] Z.W. Seh, J. Sun, Y. Sun, Y. Cui, A highly reversible room-temperature sodium metal anode, *ACS Cent. Sci.* 1 (2015) 449–455, <https://doi.org/10.1021/acscentsci.5b00328>.
- [11] L. Fan, X. Li, Recent advances in effective protection of sodium metal anode, *Nano Energy*. 53 (2018) 630–642, <https://doi.org/10.1016/j.nanoen.2018.09.017>.
- [12] D. Ruiz-Martínez, A. Kovacs, R. Gómez, Development of novel inorganic electrolytes for room temperature rechargeable sodium metal batteries, *Energy Environ. Sci.* 10 (2017) 1936–1941, <https://doi.org/10.1039/c7ee01735a>.
- [13] H. Wang, C. Wang, E. Matios, W. Li, Facile stabilization of the sodium metal anode with additives: unexpected key role of sodium polysulfide and adverse effect of sodium nitrate, *Angew. Chemie - Int. Ed.* 57 (2018) 7734–7737, <https://doi.org/10.1002/anie.201801818>.
- [14] A. Meitav, Solid electrolyte interphase (SEI) electrode, *J. Electrochem. Soc.* 128 (1981) 825, <https://doi.org/10.1149/1.2127512>.
- [15] Y. Wang, Y. Wang, Y.X. Wang, X. Feng, W. Chen, X. Ai, H. Yang, Y. Cao, Developments and perspectives on emerging high-energy-density sodium-metal batteries, *Chem.* 5 (2019) 2547–2570, <https://doi.org/10.1016/j.chempr.2019.05.026>.
- [16] J. Lee, J. Kim, S. Kim, C. Jo, J. Lee, A review on recent approaches for designing the SEI layer on sodium metal anodes, *Mater. Adv.* 1 (2020) 3143–3166, <https://doi.org/10.1039/d0ma00695e>.
- [17] Z. Yu, Y. Cui, Z. Bao, Design principles of artificial solid electrolyte interphases for lithium-metal anodes, *Cell Reports Phys. Sci.* 1 (2020) 100119, <https://doi.org/10.1016/j.xcrp.2020.100119>.

- [18] D. Li, Y. Sun, M. Li, X. Cheng, Y. Yao, F. Huang, S. Jiao, M. Gu, X. Rui, Z. Ali, C. Ma, Z.S. Wu, Y. Yu, Rational design of an artificial SEI: alloy/solid electrolyte hybrid layer for a highly reversible Na and K metal anode, *ACS Nano*. 16 (2022) 16966–16975, <https://doi.org/10.1021/acsnano.2c07049>.
- [19] A. Hu, W. Chen, X. Du, Y. Hu, T. Lei, H. Wang, L. Xue, Y. Li, H. Sun, Y. Yan, J. Long, C. Shu, J. Zhu, B. Li, X. Wang, J. Xiong, An artificial hybrid interphase for an ultrahigh-rate and practical lithium metal anode, *Energy Environ. Sci.* 14 (2021) 4115–4124, <https://doi.org/10.1039/d1ee00508a>.
- [20] B. Lee, E. Paek, D. Mitlin, S.W. Lee, Sodium metal anodes: emerging solutions to dendrite growth, *Chem. Rev.* 119 (2019) 5416–5460, <https://doi.org/10.1021/acs.chemrev.8b00642>.
- [21] R. Ponraj, J.H. Yun, J.E. Wang, X. Chen, D.J. Kim, D.K. Kim, Regulating lithium metal interface using seed-coating layer for high-power batteries, *Chem. Eng. J.* 433 (2022) 134380, <https://doi.org/10.1016/j.cej.2021.134380>.
- [22] X. Zheng, C. Bommier, W. Luo, L. Jiang, Y. Hao, Y. Huang, Sodium metal anodes for room-temperature sodium-ion batteries: applications, challenges and solutions, *Energy Storage Mater.* 16 (2019) 6–23, <https://doi.org/10.1016/j.ensm.2018.04.014>.
- [23] K. Lim, B. Fenk, K. Küster, T. Acartürk, J. Weiss, U. Starke, J. Popovic, J. Maier, Influence of porosity of sulfide-based artificial solid electrolyte interphases on their performance with liquid and solid electrolytes in Li and Na metal batteries, *ACS Appl. Mater. Interfaces*. 14 (2022) 16147–16156, <https://doi.org/10.1021/acsaami.1c23923>.
- [24] J. Yi, D. Zhou, Y. Liang, H. Liu, H. Ni, L.Z. Fan, Enabling high-performance all-solid-state lithium batteries with high ionic conductive sulfide-based composite solid electrolyte and ex-situ artificial SEI film, *J. Energy Chem.* 58 (2021) 17–24, <https://doi.org/10.1016/j.jechem.2020.09.038>.
- [25] Y. Lu, C.Z. Zhao, H. Yuan, X.B. Cheng, J.Q. Huang, Q. Zhang, Critical current density in solid-state lithium metal batteries: mechanism, influences, and strategies, *Adv. Funct. Mater.* 31 (2021) 1–33, <https://doi.org/10.1002/adfm.202009925>.
- [26] J. Huang, K. Wu, G. Xu, M. Wu, S. Dou, C. Wu, Recent progress and strategic perspectives of inorganic solid electrolytes: fundamentals, modifications, and applications in sodium metal batteries, *Chem. Soc. Rev.* 52 (2023) 4933–4995, <https://doi.org/10.1039/d2cs01029a>.
- [27] E. Matios, H. Wang, C. Wang, W. Li, Enabling safe sodium metal batteries by solid electrolyte interphase engineering: a review, *Ind. Eng. Chem. Res.* 58 (2019) 9758–9780, <https://doi.org/10.1021/acs.iecr.9b02029>.
- [28] Y. Zhao, J. Liang, Q. Sun, L.V. Goncharova, J. Wang, C. Wang, K.R. Adair, X. Li, F. Zhao, Y. Sun, R. Li, X. Sun, In situ formation of highly controllable and stable Na₃PS₄ as a protective layer for Na metal anode, *J. Mater. Chem. A* 7 (2019) 4119–4125, <https://doi.org/10.1039/c8ta10174d>.
- [29] Q. Pang, X. Liang, A. Shyamsunder, L.F. Nazar, An in vivo formed solid electrolyte surface layer enables stable plating of Li metal, *Joule*. 1 (2017) 871–886, <https://doi.org/10.1016/j.joule.2017.11.009>.
- [30] Z. Xu, J. Yang, T. Zhang, L. Sun, Y. Nuli, J. Wang, S. Ichi Hirano, Stable Na metal anode enabled by a reinforced multistructural SEI layer, *Adv. Funct. Mater.* 29 (2019) 1901924, <https://doi.org/10.1002/adfm.201901924>.
- [31] B.K. Ganesan, M. Moorthy, R. Thangavel, K.W. Nam, V. Aravindan, Y.S. Lee, Fluorine substitution enabled superior performance of Na_xMn_{2-x}O_{1.5}F_{0.5} (x = 1.05–1.3) type Na-rich cathode, *Chem. Eng. J.* 454 (2023) 139876, <https://doi.org/10.1016/j.cej.2022.139876>.
- [32] S. Amareesh, K. Karthikeyan, K.J. Kim, Y.G. Lee, Y.S. Lee, Aluminum based sulfide solid lithium ionic conductors for all solid state batteries, *Nanoscale*. 6 (2014) 6661–6667, <https://doi.org/10.1039/c4nr00804a>.
- [33] A. Wang, S. Kadam, H. Li, S. Shi, Y. Qi, Review on modeling of the anode solid electrolyte interphase (SEI) for lithium-ion batteries, *Npj Comput. Mater.* 4 (2018), <https://doi.org/10.1038/s41524-018-0064-0>.
- [34] S. Xiong, Z. Liu, H. Rong, H. Wang, M. McDaniel, H. Chen, Na₃SbSe₄-x S x as sodium superionic conductors, *Sci. Rep.* 8 (2018) 2–8, <https://doi.org/10.1038/s41598-018-27301-8>.
- [35] X. Liang, Q. Pang, I.R. Kochetkov, M.S. Sempere, H. Huang, X. Sun, L.F. Nazar, A facile surface chemistry route to a stabilized lithium metal anode, *Nat. Energy*. 2 (2017) 1–7, <https://doi.org/10.1038/nenergy.2017.119>.
- [36] K. Chen, H. Huang, S. Xu, Z. Yuan, Y. Yang, Y. Yao, X. Zhang, X. Rui, Y. Yu, Durable sodium iodide interphase stabilizing sodium metal anodes, *Carbon Neutrality*. 3 (2024), <https://doi.org/10.1007/s43979-024-00082-y>.
- [37] L. Cao, J. Guo, Y. Feng, Y. Li, Y. Qiu, W. Zhu, Y. Tan, C. Sun, X. Rui, H. Geng, A rooted multifunctional heterogeneous interphase layer enabled by surface-reconstruction for highly durable sodium metal anodes, *Adv. Funct. Mater.* 2313962 (34) (2024) 2313962, <https://doi.org/10.1002/adfm.202313962>.
- [38] H. Liu, X.B. Cheng, J.Q. Huang, S. Kaskel, S. Chou, H.S. Park, Q. Zhang, Alloy anodes for rechargeable alkali-metal batteries: progress and challenge, *ACS Mater. Lett.* 1 (2019) 217–229, <https://doi.org/10.1021/acsmaterialslett.9b00118>.
- [39] L.J. Jhang, D. Wang, A. Silver, X. Li, D. Reed, D. Wang, Stable all-solid-state sodium-sulfur batteries for low-temperature operation enabled by sodium alloy anode and confined sulfur cathode, *Nano Energy*. 105 (2023) 107995, <https://doi.org/10.1016/j.nanoen.2022.107995>.
- [40] L. Schafzahl, H. Ehmman, M. Kriechbaum, J. Sattelkow, T. Ganner, H. Plank, M. Wilkening, S.A. Freunberger, Long-chain Li and Na alkyl carbonates as solid electrolyte interphase components: structure, ion transport, and mechanical properties, *Chem. Mater.* 30 (2018) 3338–3345, <https://doi.org/10.1021/acs.chemmater.8b00750>.
- [41] H. Gao, S. Xin, L. Xue, J.B. Goodenough, Stabilizing a high-energy-density rechargeable sodium battery with a solid electrolyte, *Chem.* 4 (2018) 833–844, <https://doi.org/10.1016/j.chempr.2018.01.007>.
- [42] B. Sun, P. Li, J. Zhang, D. Wang, P. Munroe, C. Wang, P.H.L. Notten, G. Wang, Dendrite-free sodium-metal anodes for high-energy sodium-metal batteries, *Adv. Mater.* 30 (2018) 1–8, <https://doi.org/10.1002/adma.201801334>.
- [43] X. Lv, F. Tang, Y. Yao, C. Xu, D. Chen, L. Liu, Y. Feng, X. Rui, Y. Yu, Sodium–gallium alloy layer for fast and reversible sodium deposition, *SusMat.* 2 (2022) 699–707, <https://doi.org/10.1002/sus2.97>.
- [44] M. Zhu, G. Wang, X. Liu, B. Guo, G. Xu, Z. Huang, M. Wu, H. Liu, S. Dou, C. Wu, Dendrite-free sodium metal anodes enabled by a sodium benzenedithiolate-rich protection layer, *Angew. Chemie*. 132 (2020) 6658–6662, <https://doi.org/10.1002/ange.201916716>.
- [45] M. Bai, K. Zhang, D. Du, X. Tang, Y. Liu, H. Wang, M. Zhang, S. Liu, Y. Ma, SnSb binary alloy induced heterogeneous nucleation within the confined nanospace: Toward dendrite-free, flexible and energy/power dense sodium metal batteries, *Energy Storage Mater.* 42 (2021) 219–230, <https://doi.org/10.1016/j.ensm.2021.07.032>.
- [46] L. Wang, J. Shang, Q. Huang, H. Hu, Y. Zhang, C. Xie, Y. Luo, Y. Gao, H. Wang, Z. Zheng, Smoothing the sodium-metal anode with a self-regulating alloy interface for high-energy and sustainable sodium-metal batteries, *Adv. Mater.* 33 (2021) 1–11, <https://doi.org/10.1002/adma.202102802>.
- [47] Lary E. Rush, Jr., Zachary D. Hood, N.A.W. Holzwarth, Unraveling the electrolyte properties of Na₃SbS₄ through computation and experiment, *Phys. Rev. Mater.* 1 (2021) 075405, <https://doi.org/10.1103/PhysRevMaterials.1.075405>.
- [48] H. Yu, D. Jiang, X. Cheng, P. Lu, S. Li, H. Zhang, Y. Jiang, F. Huang, Ultrastable sodium/potassium metal anode enabled by a multifunctional interphase layer with enhanced ion transport kinetics, *Adv. Funct. Mater.* 33 (2023) 1–10, <https://doi.org/10.1002/adfm.202307628>.
- [49] Y. Shuai, J. Lou, X. Pei, C. Su, X. Ye, L. Zhang, Y. Wang, Z. Xu, P. Gao, S. He, Z. Wang, K. Chen, Constructing an in situ polymer electrolyte and a Na-rich artificial SEI layer toward practical solid-state Na metal batteries, *ACS Appl. Mater. Interfaces*. 14 (2022) 45382–45391, <https://doi.org/10.1021/acsaami.2c12518>.
- [50] G. Li, X. Lou, C. Peng, C. Liu, W. Chen, Interface chemistry for sodium metal anodes/batteries: a review, *Chem. Synth.* 2 (2022), <https://doi.org/10.20517/cs.2022.19>.
- [51] Z. Luo, S. Tao, Y. Tian, L. Xu, Y. Wang, X. Cao, Y. Wang, W. Deng, G. Zou, H. Liu, H. Hou, X. Ji, Robust artificial interlayer for columnar sodium metal anode, *Nano Energy*. 97 (2022) 107203, <https://doi.org/10.1016/j.nanoen.2022.107203>.
- [52] W. Luo, C.F. Lin, O. Zhao, M. Noked, Y. Zhang, G.W. Rubloff, L. Hu, Ultrathin surface coating enables the stable sodium metal anode, *Adv. Energy Mater.* 7 (2017) 1–6, <https://doi.org/10.1002/aenm.201601526>.
- [53] M. Mandl, J. Becherer, D. Kramer, R. Mönig, T. Diemant, R.J. Behm, M. Hahn, O. Böse, M.A. Danzer, Sodium metal anodes: deposition and dissolution behaviour and SEI formation, *Electrochim. Acta*. 354 (2020) 2019, <https://doi.org/10.1016/j.jelectacta.2020.136698>.
- [54] M. Moorthy, B. Moorthy, B.K. Ganesan, A. Saha, S. Yu, D.H. Kim, S. Hong, S. Park, K. Kang, R. Thangavel, Y.S. Lee, A series of hybrid multifunctional interfaces as artificial SEI layer for realizing dendrite free, and long-life sodium metal anodes, *Adv. Funct. Mater.* 33 (2023) 2300135, <https://doi.org/10.1002/adfm.202300135>.
- [55] X. Zhou, F. Liu, Y. Wang, Y. Yao, Y. Shao, X. Rui, F. Wu, Y. Yu, Heterogeneous interfacial layers derived from the in situ reaction of CoF₂ nanoparticles with sodium metal for dendrite-free Na metal anodes, *Adv. Energy Mater.* 12 (2022) 1–9, <https://doi.org/10.1002/aenm.202202323>.
- [56] B. Sayahpour, W. Li, S. Bai, B. Lu, B. Han, Y.T. Chen, G. Deysher, S. Parab, P. Ridley, G. Raghavendran, L.H.B. Nguyen, M. Zhang, Y.S. Meng, Quantitative analysis of sodium metal deposition and interphase in Na metal batteries, *Energy Environ. Sci.* 17 (2024) 1216–1228, <https://doi.org/10.1039/d3ee03141a>.
- [57] J. Xie, Z. Li, X. Zheng, F. Tian, D. Lei, C. Wang, Built-in electric field of in situ formed artificial interface layer induces fast and uniform sodium-ions transmission to achieve a long-term stable sodium metal battery under harsh conditions, *Adv. Funct. Mater.* 2315309 (34) (2024) 2314954, <https://doi.org/10.1002/adfm.202315309>.
- [58] S. Xia, W. Fan, Z. Hou, C. Li, Z. Jiang, J. Yang, J. Mao, S. Zheng, Fast ion transport interphase integrated with space confinement enabling high-rate and long-lifespan na metal batteries, *Adv. Funct. Mater.* 2314954 (2024) 1–9, <https://doi.org/10.1002/adfm.202314954>.
- [59] H. Shi, Y. Zhang, Y. Liu, C. Yuan, Metallic sodium anodes for advanced sodium metal batteries: progress, challenges and perspective, *Chem. Rec.* 22 (2022), <https://doi.org/10.1002/tcr.202200112>.
- [60] S. Zhang, Y. Zhao, F. Zhao, L. Zhang, C. Wang, X. Li, J. Liang, W. Li, Q. Sun, C. Yu, J. Luo, K. Doyle-Davis, R. Li, T.K. Sham, X. Sun, Gradiently sodiated alucone as an interfacial stabilizing strategy for solid-state Na metal batteries, *Adv. Funct. Mater.* 30 (2020) 1–9, <https://doi.org/10.1002/adfm.202001118>.
- [61] W. Wang, H. Sun, Hu. Shan, Z. Jian, W. Chen, High current and dendrite-tolerant NaF/ZnO coated Na₃Zr₂Si₂PO₁₂ electrolyte prepared by a facile spraying method, *Solid State Ion.* 411 (2024) 116577, <https://doi.org/10.1016/j.ssi.2024.116577>.
- [62] Guangmei Hou, Xiaoxin Ma, Qidi Sun, Qing Ai, Xiaoyan Xu, Lina Chen, Deping Li, Jinghua Chen, Hai Zhong, Yang Li, Zhibin Xu, Pengchao Si, Jinkui Feng, LinZhang, Fei Ding, and Lijie Ci, Lithium Dendrite suppression and enhanced interfacial compatibility enabled by an Ex Situ SEI on Li anode for lagp-based all-solid-state batteries, *ACS Appl. Mater. Interfaces* 10 (2018) 18610–18618, <https://doi.org/10.1021/acsaami.8b01003>.